

April 2007

Nanoscale mechanisms of misfit dislocation propagation in undulated Si_{1-x}Gex/Si(100) epitaxial thin films

Chi-Chin Wu
University of Virginia

Eric A. Stach
School of Materials Engineering and Birck Nanotechnology Center, Purdue University, eastach@purdue.edu

Robert Hull
University of Virginia

Follow this and additional works at: <http://docs.lib.purdue.edu/nanopub>

Wu, Chi-Chin; Stach, Eric A.; and Hull, Robert, "Nanoscale mechanisms of misfit dislocation propagation in undulated Si_{1-x}Gex/Si(100) epitaxial thin films" (2007). *Birck and NCN Publications*. Paper 25.
<http://docs.lib.purdue.edu/nanopub/25>

This document has been made available through Purdue e-Pubs, a service of the Purdue University Libraries. Please contact epubs@purdue.edu for additional information.

Nanoscale mechanisms of misfit dislocation propagation in undulated $\text{Si}_{1-x}\text{Ge}_x/\text{Si}(100)$ epitaxial thin films

Chi-Chin Wu¹, Eric A Stach² and Robert Hull¹

¹ Department of Materials Science and Engineering, 395 McCormick Road, University of Virginia, Charlottesville, VA 22904, USA

² School of Materials Engineering and Birck Nanotechnology Center, 501 Northwestern, Purdue University, West Lafayette, IN 47907, USA

E-mail: cw9r@virginia.edu

Received 5 January 2007, in final form 8 February 2007

Published 23 March 2007

Online at stacks.iop.org/Nano/18/165705

Abstract

Nanoscale lateral variations in the stress field of undulated $\text{Si}_{0.7}\text{Ge}_{0.3}/\text{Si}(100)$ films have been experimentally studied via *in situ* transmission electron microscopy annealing and through finite element calculations. When annealed at $\sim 480^\circ\text{C}$, misfit dislocations in a 30 nm film (having surface undulations of ~ 70 nm wavelength and ~ 3 nm amplitude) propagated at 80 nm s^{-1} average speed but with periodic variations from $0\text{--}30\text{ nm s}^{-1}$ at the peaks of the undulations to $160\text{--}240\text{ nm s}^{-1}$ at the troughs. A 2.0 GPa average film stress with variations from 3.2 to 4.4 GPa at the troughs to 0.7–1.2 GPa at the peaks is inferred from the observed dislocation velocities. These stress variations are significantly higher than those calculated from a finite element model of $\text{Si}_{0.7}\text{Ge}_{0.3}/\text{Si}$ with the same surface geometry. Using standard models of dislocation kink dynamics, we have calculated how the effect of high stresses at the undulation troughs would be expected to enhance kink nucleation rates, and have found good agreement between our models and the experimentally observed range of dislocation velocities. These observations demonstrate the potential of probing the nanoscale structure in thin films through local variations of dislocation velocities.

1. Introduction

For heteroepitaxial structures grown under kinetically limited conditions, a compressively strained coherent film often roughens after a characteristic thickness to help release the stored elastic strain energy. Such morphological instability has been widely studied for the growth of lattice-mismatched heteroepitaxial thin films (e.g. [1–5]). A roughened surface is able to reduce the overall film stress by locally redistributing the stress field such that the film is more compressed at troughs and less compressed at peaks. Although surface roughening has long been recognized as one of the fundamental processes during heteroepitaxial growth, thus far only the macroscopic net stress change has been quantitatively measured for low misfit $\text{Si}_{1-x}\text{Ge}_x/\text{Si}(100)$ [6]. Relatively little is known

experimentally about the quantitative variations of stress field underneath the roughened free surface for low misfit heteroepitaxial thin films even though local stress variations have been experimentally explored (e.g. [7]).

An additional strain relief mechanism is that misfit dislocations nucleate and propagate after a strained heteroepitaxial film grows above a critical thickness [8]. For strained heteroepitaxial thin films, the dynamics of misfit dislocation motion is dependent on the net stress acting on the dislocation (the effective or excess stress, σ_{ex} , originally developed by Alexander and Haasen [9] for bulk diamond structures. This excess stress is given by [10]:

$$\sigma_{\text{ex}} = \sigma_s - \sigma_T \quad (1)$$

where σ_s is the resolved local misfit stress and σ_T is the line tension, as shown in figure 1. For $\text{Si}_{1-x}\text{Ge}_x/\text{Si}(100)$,

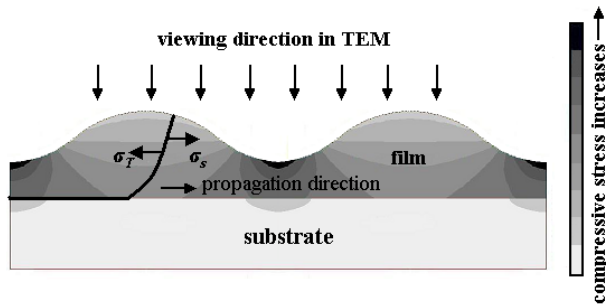


Figure 1. Schematic diagram showing the stress fields experienced by a propagating dislocation cutting through undulations in a strained heteroepitaxial thin film.

dislocation dynamics have already been extensively studied and correlated to the effective stress by several groups [11–16]. In our previous work [14], the following relationship was established between measured misfit dislocation velocity (v_m) and stress:

$$v^* = v_m \sigma_{\text{ex}}^{-1} e^{-0.6x/kT} \quad (\text{m s}^{-1} \text{ Pa}^{-1}) \quad (2)$$

where

$$v^* = e^{-(7.8 \pm 1.4)} e^{-(2.03 \pm 0.1 \text{ eV})/kT} \quad (\text{m s}^{-1} \text{ Pa}^{-1}) \quad (3)$$

here v^* is the velocity normalized to an equivalent velocity at 1 Pa in pure Si, and x is the average Ge concentration in the film. In equation (2), the exponential term accounts for the 0.6 eV difference in the glide activation energy between pure Si and Ge [9]. In this work we will use this relationship between v_m and σ_{ex} as a tool for nanoscale stress measurement, by exploring correlations between local dislocation velocity determined by observations *in situ* in the transmission electron microscope (TEM) and the calculated stress variations arising from local surface morphology.

2. Experimental and simulation details

The results presented in this paper are from a $\text{Si}_{0.7}\text{Ge}_{0.3}/\text{Si}(100)$ structure with a 30 nm mean film thickness and surface undulations of ~ 70 nm wavelength and ~ 3 nm amplitude, grown by molecular beam epitaxy at 525°C and 1 \AA s^{-1} growth rate. As grown this film has a very low dislocation density due to the sluggish dislocation kinetics that exist in this system under these growth conditions [13, 14], and most of the lattice mismatch stress in the film is retained. Thus on annealing *in situ* in the TEM, further dislocation propagation occurs, driven by the local excess stress in the film.

Plan-view (electron beam parallel to the $\text{Si}_{0.7}\text{Ge}_{0.3}/\text{Si}$ interface normal) TEM specimens were prepared by backside chemical etching with successive solutions containing different ratios of HNO_3 , HF , and CH_3COOH (4:1:2, 10:1:0, and 15:1:0, respectively) and studied in a JEOL 2000FX TEM operated at 200 keV. Under TEM diffraction contrast imaging conditions, figure 2(a), the as-grown sample reveals strong strain contrast from surface undulations and has relatively few misfit dislocations visible in the overall field of view of about $10\text{--}100 \mu\text{m}^2$. A corresponding $1 \mu\text{m} \times 1 \mu\text{m}$

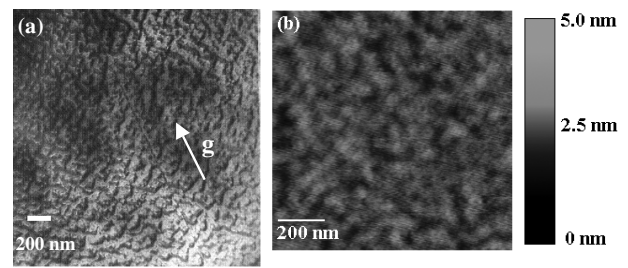


Figure 2. Undulated $\text{Si}_{0.7}\text{Ge}_{0.3}$ film grown at 525°C and 1 \AA s^{-1} growth rate: (a) Plan view bright field TEM image, $g = (022)$, (b) $1 \mu\text{m} \times 1 \mu\text{m}$ AFM scan (the edge of the AFM image is approximately parallel to the $\langle 011 \rangle$ direction).

atomic force microscopy (AFM) scan (Dimension 3100, DI Digital Instruments, tapping mode), is shown in figure 2(b). A relatively thick sample region (about several hundred nanometres thick) at least several microns distance away from the thin foil edge was observed in TEM to minimize possible thin foil relaxation effects [17]. The sample was gradually heated and the temperature was measured by a Pt/Rh thermocouple welded to the heating stage. (Although there may be discrepancies between the indicated and actual temperatures of the observed field in the specimen, temperature calibration is not critical in this work because all of the measurements were performed at a constant temperature.) The typical beam current density for these observations was of the order of $\sim 10^{-1} \text{ A cm}^{-2}$ on the specimen. Reports in the literature show that electron beam irradiation does not significantly affect dislocation motion in Si at these irradiation densities and sample temperatures [18, 19]. A misfit dislocation was selected in the field of view and its threading arm was observed while heating to progressively higher temperatures until dislocation movement was observed. The resulting dislocation propagation dynamics were recorded onto a videotape in real time for quantitative analysis. The spatial distance of dislocation propagation was measured by reference to fiduciary features (e.g. distinguishing topographical features or specks of contamination) in the images. The dislocation velocity was calculated by taking the increment of the distance data with respect to time between each video frame ($1/30 \text{ s}$ interval). The Fourier transform of the dislocation velocity and the surface topography data was calculated using the commercial statistics software package SYSTAT version 11 (SYSTAT Software, Inc.)³.

The finite element calculations of the film stress field were carried out using an elastically-isotropic model with the commercial software package ANSYS⁴. In the model, the undulated $\text{Si}_{0.7}\text{Ge}_{0.3}/\text{Si}$ thin film was constructed as having a periodic sinusoidal surface of 70 nm wavelength and 3 nm amplitude with a mean film thickness of 30 nm, i.e. the same as those observed experimentally. The lateral dimension of the model was equivalent to one-half of the undulation wavelength due to symmetry. The compressive stresses induced by the lattice mismatch at the interface between the $\text{Si}_{0.7}\text{Ge}_{0.3}$

³ SYSTAT Software Inc., 501 Canal Boulevard, Suite E, Point Richmond, CA 94804-2028, USA (www.systat.com).

⁴ ANSYS Inc., Southpointe, 275 Technology Drive, Canonsburg, PA 15317, USA (www.anays.com).

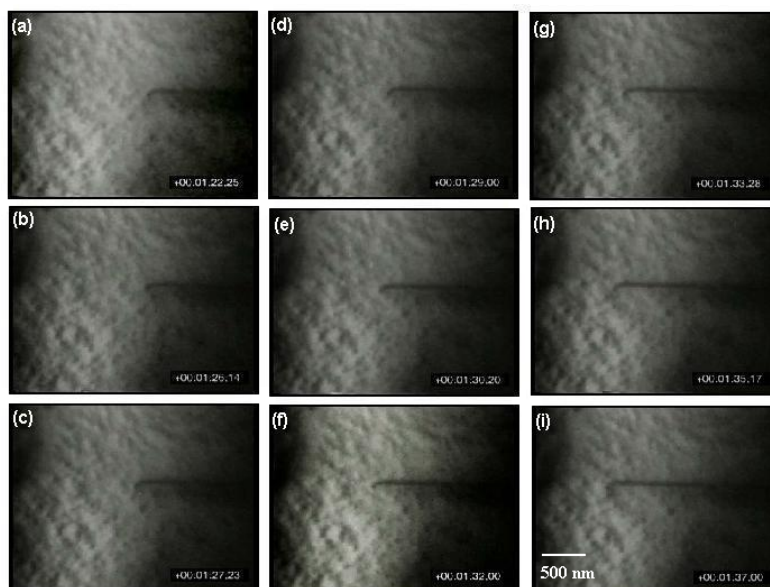


Figure 3. Video sequence of 40000 \times magnification showing propagation of the observed dislocation annealed at $\sim 480^\circ\text{C}$. The overall duration from (a) to (i) was ~ 15 s.

Table 1. Materials constants used in the finite element model [20].

	Si(100)	Si _{0.7} Ge _{0.3} film
Lattice spacing (\AA)	5.43	5.50
Modulus of elasticity (GPa)	165.92	156.51
Poisson's ratio	0.22	0.21

epitaxial film and the Si substrate were generated in the model by applying an initial temperature load to suitably scaled thermal expansion coefficients of the film and the substrate. Both the Si_{0.7}Ge_{0.3} epitaxial film and the Si substrate (to a thickness of 100 nm) are included in the calculations. For the epitaxial film, the lattice constant and isotropic elastic constants were derived from those of bulk Si and Ge by interpolating linearly to the film composition of 30% Ge, as shown in table 1. The boundary conditions in the model were such that no displacement was allowed in all directions at the bottom edge of the Si substrate and in the axial directions for the edges of the entire model. The top surface of the film is free to relax in all directions.

3. Results

The propagation of the observed misfit dislocations was typically discernible at $\sim 480^\circ\text{C}$ at 40 000 \times magnification in the TEM. Figure 3 represents a portion of the recorded video sequence illustrating dislocation movement. After analysing the dynamics of the dislocation from the recorded video sequence, we found that the dislocation propagation velocity varied periodically with a spatial repeat of ~ 50 nm. The maximum dislocation propagation velocity reached as high as 160–240 nm s^{-1} and as low as 0–30 nm s^{-1} (presumably at film troughs and peaks where the local stresses are highest and lowest, respectively), with an average velocity of ~ 80 nm s^{-1} , as shown in figure 4. From equations (2) and (3), it is apparent

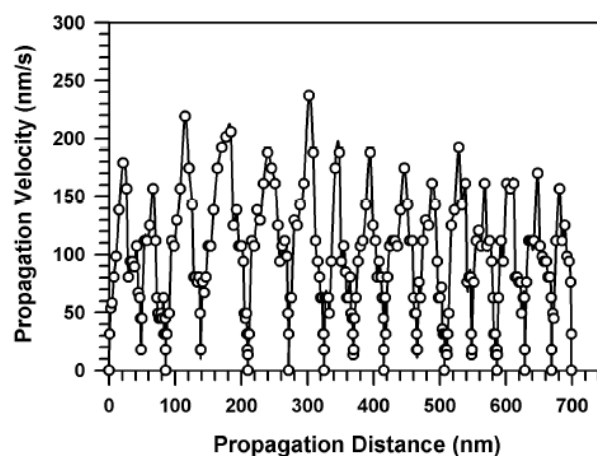


Figure 4. Dislocation propagation velocity versus propagation distance at 480°C .

that the dislocation propagation velocity is proportional to σ_{ex} which is directly correlated to the misfit stress through equation (1) and the following equations:

$$\sigma = \frac{2G\varepsilon(1+\nu)}{(1-\nu)} = \frac{\sigma_s}{(\cos\varphi \times \cos\lambda)} \quad (4)$$

and

$$\sigma_T = \frac{Gb \cos\varphi(1-\nu \cos^2\theta)}{4\pi h(1-\nu)} \ln\left(\frac{ah}{b}\right). \quad (5)$$

Here σ is the stress generated by the lattice mismatch strain ε , φ is the angle between the interface normal and the glide plane, λ is the angle between the Burgers vector and a line in the interface drawn normal to the dislocation line direction. Here $\cos\varphi$ and $\cos\lambda$ are 0.82 and 0.50, respectively. The line tension in equation (5) is calculated from standard equations for dislocation self-energy [21]. Here, G is the

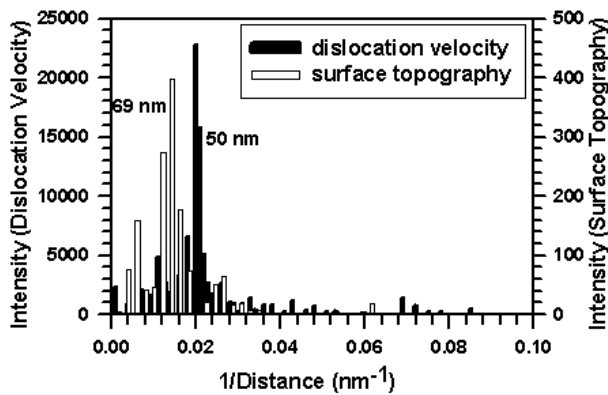


Figure 5. Fourier spectra of dislocation velocities determined by *in situ* TEM and surface topography measured by AFM.

shear modulus (65 GPa), b is the magnitude of Burger's vector (0.39 nm), ν is the Poisson's ratio (0.21), θ is the angle between the dislocation line and the Burger's vector (60°), α is a factor describing the dislocation core energy (using 4 here for covalent semiconductors [21]), and h is the film thickness. For the film geometry and composition studied here, the line tension is typically an order of magnitude smaller than the misfit stress so that the magnitude of excess stress, σ_{ex} , driving the dislocation motion is mainly controlled by the misfit stress, σ (we do explicitly include the line tension in the subsequent analysis however). Therefore, it appears that, as anticipated, the enhanced compressive stress at troughs causes an increase in dislocation velocity at these regions. On the other hand, the reduced misfit stress at peaks apparently causes the dislocation to slow down.

Correlation of the surface morphology to the variations in dislocation velocity is also demonstrated by Fourier transform analysis, figure 5. Here, the Fourier spectrum from dislocation velocities shows a maximum at a frequency corresponding to ~ 50 nm in real space, corresponding within a factor of two to the peak centred around a real space distance of 70 nm in the Fourier spectrum of the surface topography. (We note that

the misfit dislocation propagation is along the $\langle 011 \rangle$ direction while the surface undulations are typically along the $\langle 001 \rangle$ direction for this sample, therefore there is a $\sqrt{2}$ geometrical relationship between periodicities in these two directions.)

Variations in σ_{ex} can be deduced from the variations in measured dislocation velocities by equations (2) and (3). By substituting the line tensions, σ_T , calculated from equation (5), into equation (1) and applying the relation of equation (4), local compressive stresses, σ , can be obtained as being in the ranges of 3.2–4.4 GPa and 0.7–1.2 GPa in the regions under the surface troughs and peaks, respectively, with an average over the entire film of 2.0 GPa.

Figure 6(a) shows the contours of the stress component σ_{xx} (equivalent to the unresolved applied stress on the dislocation, σ). The x and y directions in the model are defined as those perpendicular and parallel to the growth directions, respectively. Figure 6(b) shows the lateral profiles of both the average of this compressive stress component and the stresses at the top surface as a function of position along the undulation wavelength, calculated from the finite element model. The average stress profile is determined by averaging the local stresses σ_{xx} through the thickness of the film in columns under the appropriate location along the surface wave from peak to trough. These average misfit stresses vary from 2.34 GPa at the peaks to 2.61 GPa at the troughs, with a 2.46 GPa mean value over the entire film. These calculated stress variations are thus significantly smaller than those inferred by the *in situ* TEM measurements of dislocation propagation velocity.

4. Discussion

Discrepancies between the local stress variations inferred by our experimentally-measured dislocation velocities and those calculated via the FEM model suggest that there must be other mechanisms operating to cause the large observed variations in dislocation velocity. One mechanism to consider is lateral composition variations between peaks and troughs, which can occur as a result of the larger lattice parameter Ge atoms preferring to segregate to the peak regions where bond lengths are locally more relaxed [3, 22]. However, this would

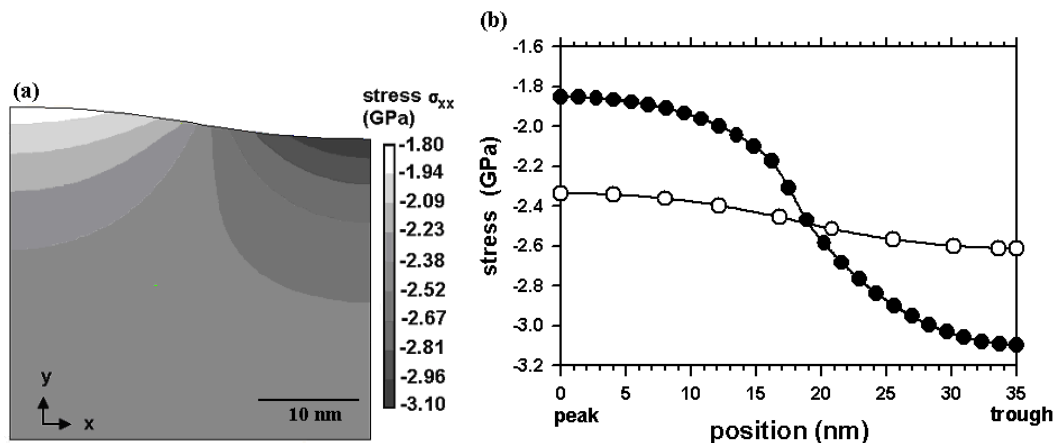


Figure 6. Isotropic FEM model of a 30 nm $\text{Si}_{0.7}\text{Ge}_{0.3}$ film having surface undulations of 70 nm wavelength and 3 nm amplitude (the substrate is not shown but is included in the calculation, as described in the text): (a) compressive stress distributions, (b) profiles of the average stresses (open circles) and the stress at the top surface (solid circles) along the lateral direction of undulation. The negative values represent compressive stresses.

actually serve to *reduce* variations in dislocation velocity, as the segregation reduces the stress variations between peaks and troughs and because the resultant higher Ge concentration at the peaks would serve to accelerate dislocations at the peaks and decelerate them at the troughs (equation (2)), thus further reducing the variation in dislocation velocities.

Another possible mechanism to consider is local stress enhancements due to steps at the interface between the film surface and its native oxide, as we have previously considered [23]. However, so far as we can tell from AFM and cross-sectional TEM images, the curvature at troughs and peaks are similar, and thus the step densities should be similar at both. Thus while this effect could cause a net uniform enhancement in dislocation velocity, it should not cause a substantial *variation* in velocity between peaks and troughs, as we observe.

A final possibility we have considered is the stress dependence of single-kink nucleation at the film surface [13, 21, 23], as shown in figure 7.

In the single-kink nucleation model, the critical kink separation distance S_o^* between the kink itself and its image is given by:

$$S_o^* = \sqrt{\frac{Gbq(1+\nu)}{8\pi\sigma_s(1-\nu)}} \quad (6)$$

where q is the distance between Peierl's valleys (3.3 Å). Our finite element model showed that the film has a minimum stress of 1.85 GPa right at the surface of the morphological peaks (as opposed to the earlier 'average' value in figure 6 that was determined from a column spanning the entire thickness of the film below the peak) and 3.10 GPa maximum at the surface of troughs, with a mean stress at the surface of 2.41 GPa. From these stresses, we calculated S_o^* through equation (6) and determined that the average critical kink-kink separation distance is ~ 7 Å (by taking the average of the calculated values of 8 Å at peaks and 6 Å at troughs) for this sample. (More precisely, as shown in figure 7, we consider half of S_o^* as the range of depth for single-kink nucleation at the film surface and calculated the average stresses within this range. This generates average stresses of 1.87 GPa at peaks and 3.08 GPa at troughs, which is actually a very small correction to the surface values.) Using these average stresses we calculated the single-kink formation energy F'_k and nucleation rate J_k by the following equations [13, 21, 23]:

$$F'_k = F_k - \sqrt{\frac{(1+\nu)G\sigma_s q^3 b^3}{8\pi(1-\nu)}} \quad (7)$$

$$J_k = \frac{\nu_D q b S_o^* \sigma_{ex}}{4kT} \exp\left[\frac{-(E_m + 2F'_k)}{kT}\right] \quad (8)$$

where F_k is the stress-free activation energy for single-kink nucleation (taken here to be 0.7 eV) [24], E_m is the kink migration energy (1.36 eV, calculated by linear interpolation for $x = 0.3$ in $\text{Ge}_x\text{Si}_{1-x}$ assuming E_m to be 1.55 eV for Si and 0.9 eV for Ge [25]), and ν_D is the kink attempt jump frequency (approximated here by the Debye frequency $1.3 \times 10^{13} \text{ s}^{-1}$ for Si). These equations predict that the enhanced (with respect to the mean stress at the surface) compressive stress of ~ 700 MPa at trough surfaces would reduce the activation energy for single-kink nucleation F'_k by about 0.08 eV. This

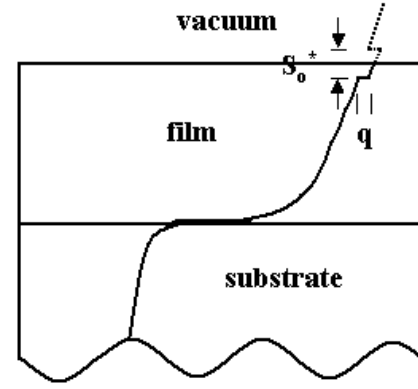


Figure 7. Schematic diagram of a single kink nucleated at a free surface. S_o^* is the critical kink-kink separation and q is the kink jump distance. The broken line in the vacuum represents the image kink and dislocation.

would increase the kink nucleation rate at troughs (with respect to a planar film) by over one order of magnitude. The reduction in stress at the surface of the peaks would reduce the kink nucleation rate and local dislocation velocity correspondingly. The calculated single-kink nucleation rates are $\sim 3000 \text{ s}^{-1}$ at troughs and $\sim 20 \text{ s}^{-1}$ at peaks. This difference in nucleation rates of two orders of magnitude between peaks and troughs would be directly translated into equivalent variations in dislocation velocity according to the relation [13]:

$$v_{sk} = J_k q \quad (9)$$

where v_{sk} is the predicted dislocation velocity based on the single-kink nucleation model. While we recognize that the elasticity methods used in the derivation of equations (7) and (8) are approximate at best at these near-atomic length scales, and that there are significant ranges in the reported values of the microscopic parameters F_k and E_m , this analysis suggests that the magnitude in variation of single-kink nucleation rates as a function of the variation in the stress at the surface is sufficient to explain our observed variations in misfit dislocation velocities.

We now relate the more complex form of equations (7)–(9) to the more phenomenological description of dislocation velocity in equations (2) and (3). The latter description is based on the standard description of dislocation glide motion in semiconductor materials (e.g. [9]):

$$v = \nu_o \sigma \exp(-E_v/kT) \quad (10)$$

here v is the dislocation glide velocity, ν_o is a prefactor, σ is the operative resolved stress acting on the dislocation (in this analysis, the excess stress, σ_{ex}) and E_v is the glide activation energy. In comparing the form of equation (10) to that of equations (7)–(9), the prefactor ν_o is represented by the material, geometrical and physical constants in the prefactor of equation (8) together with the q term in equation (9). The prefactor in equation (8) also contains a $1/T$ term that is absent in equations (2), (3) and (10); however this is greatly dominated by the exponential temperature dependence. The major difference between the two sets of equations is the stress dependence of the activation energy that is present in

equations (7)–(9) but absent in equations (2), (3) and (10). As we have previously discussed [13, 15, 23], this effect is significant at the high excess stresses that can be attained in lattice-mismatched epitaxy, and is further demonstrated here.

5. Conclusions

We have explored nanoscale stress variations associated with surface instabilities of a heteroepitaxial film by *in situ* TEM measurements of misfit dislocation velocities and compared them to those calculated via finite element modelling. For a 30 nm Si_{0.7}Ge_{0.3}/Si(100) film with undulations ~70 nm in wavelength and 3 nm in amplitude, the observed periodic variations in measured dislocation propagation velocities correlate strongly with surface morphology. By correlating the velocity data to local stresses using previously established stress–velocity correlations, the average local stresses in the film are inferred as 3.2–4.4 GPa beneath the troughs and 0.7–1.2 GPa beneath the peaks with an overall mean film stress of 2.0 GPa. These variations are substantially higher than those predicted by finite element analysis, suggesting that other mechanisms are implicated in the observed variations of misfit dislocation velocity. Calculations of the variation in single-kink nucleation rates at the film peaks and troughs support a variation in dislocation velocity that is of sufficient magnitude to explain those observed from experiments, suggesting this as a possible mechanism for the observed dislocation velocity variations. In summary, we believe that this work demonstrates that nanoscale resolution in measurement of local dislocation velocities by *in situ* TEM can provide significant insight into local stress variations and atomic-scale mechanisms of dislocation motion.

Acknowledgments

This work is funded by the NSF-MRSEC at UVa: ‘The Center for Nanoscopic Materials Design’ under DMR no. 0075116. We acknowledge Dr J C Bean for growing the sample studied in this work.

References

- [1] Srolovitz D J 1989 *Acta Metall.* **37** 621
- [2] Gao H and Nix W D 1999 *Annu. Rev. Mater. Sci.* **29** 173
- [3] Guyer J E and Voorhees P W 1996 *Phys. Rev. B* **54** 11710
Guyer J E and Voorhees P W 1998 *J. Cryst. Growth* **187** 150
- [4] Venezuela P and Tersoff J 1998 *Phys. Rev. B* **58** 10871
- [5] Spencer B J, Voorhees P W and Tersoff J 2001 *Phys. Rev. B* **64** 235318
- [6] Floro J A, Chason E, Freund L B, Twisten R D, Hwang R Q and Lucadamo G A 1999 *Phys. Rev. B* **59** 1990
- [7] Cullis A G, Robbins D J, Pidduck A J and Smith P W 1992 *J. Cryst. Growth* **123** 333
- [8] Matthews J W and Blakeslee A E 1974 *J. Cryst. Growth* **27** 118
- [9] Alexander H and Haasen P 1968 *Solid State Phys.* **22** 27
- [10] Tsao J Y, Dodson B W, Picraux S T and Cornelison D M 1987 *Phys. Rev. Lett.* **59** 2455
- [11] Tuppen C G and Gibbings C J 1990 *J. Appl. Phys.* **68** 1526
- [12] Houghton D C 1990 *Appl. Phys. Lett.* **57** 2124
- [13] Hull R, Bean J C, Bahnck D, Peticolas L J Jr and Short K T 1991 *J. Appl. Phys.* **70** 2052
- [14] Hull R, Stach E A, Tromp R, Ross F and Reuter M 1999 *Phys. Status Solidi a* **171** 133
- [15] Hull R and Bean J C 1993 *Phys. Status Solidi a* **138** 533
- [16] Wang T C, Zhang Y W and Chua S J 2001 *Acta Mater.* **49** 1599
- [17] Hull R 1993 *Appl. Phys. Lett.* **63** 2291
- [18] Yonenaga I, Werner M, Bartsch M, Messerschmidt U and Weber E R 1999 *Phys. Status Solidi a* **171** 35
- [19] Maeda K, Suzuki K, Yamashita Y and Mera Y 2000 *J. Phys.: Condens. Matter* **12** 10079
- [20] Meyers M and Chawla K K 1998 *Mechanical Behaviour of Materials* (Englewood Cliffs, NJ: Prentice-Hall) chapter 2
- [21] Hirth J P and Lothe J 1982 *Theory of Dislocations* (New York: Wiley) chapters 8 and 15
- [22] Wu C and Hull R 2006 *J. Appl. Phys.* **100** 08350
- [23] Stach E A and Hull R 2001 *Appl. Phys. Lett.* **79** 335
- [24] Kolar H R, Spence J C H and Alexander H 1996 *Phys. Rev. Lett.* **77** 4031
- [25] Maeda K, Inoue M, Suzuki K, Amasuga H, Nakamura M and Kanematsu E 1997 *J. Physique III* **7** 1451